cycloTRACK (v1.0) - Tracking winter extra-tropical cyclones based on relative vorticity: Sensitivity to data filtering and other relevant parameters

Emmanouil Flaounas (1), Vassiliki Kotroni (2), Konstantinos Lagouvardos (2), Ilias Flaounas (3)

1 LMD/IPSL, CNRS and Ecole Polytechnique, Palaiseau, France

2 Institute for Environmental Research and Sustainable Development, National Observatory of Athens, Athens, Greece

3 Intelligent Systems Laboratory, University of Bristol, Bristol, UK

Abstract

In this study we present a new cyclone identification and tracking algorithm, namely cycloTRACK. The algorithm is an iterative process and at each time step it identifies all cyclone centers. These are defined as relative vorticity maxima, embedded in smoothed enclosed contours of at least $3x10^{-5}$ s^{-1} at the atmospheric level of 850hPa. Then, the algorithm constructs the tracks by linking the different cyclone locations at consecutive time steps. In particular, for each identified cyclone center the algorithm builds all possible tracks. The final cyclone track is selected as the one that presents the minimum score of a cost function. The cost function is the average differences of relative vorticity between consecutive track points, weighted by the distance between the track points. For each cyclone, the algorithm also computes "an effective area" in which different physical diagnostics are measured such as the minimum pressure and the maximum wind speed and they are attributed to the tracked cyclones. The area size is a function of the cyclone relative vorticity.

We apply the algorithm to the ERA-Interim reanalyses in order to track the northern hemisphere extra-tropical cyclones of the 1989–2009 winters. We assess the sensitivity of our method to the relative vorticity filtering and to other parameters used to perform tracking.

1. Introduction

Identification and tracking of atmospheric features is thoroughly used in atmospheric science research. Several atmospheric features are identified and tracked in climatological datasets such as Mesoscale Convective Systems (MCS; e.g. Machado et al, 1998), conveyor belts (e.g. Eckhardt et al, 2004), cut-off lows (Wernli and Sprenger, 2007), fronts (Hewson and Titley, 2010), jet streams (Limbach et al, 2012) and dry air intrusions (Roca et al, 2005; Flaounas et al, 2012). However, tropical and extra-tropical cyclones are the most investigated atmospheric features by identification and tracking algorithms (e.g. Hodges, 1999; Blender and Schubert, 2000; Hoskins and Hodges 2002; Ulbrich et al, 2009; Inatsu, 2009).

Typical methods for cyclone detection and tracking utilize a two-step approach: First they identify the location of cyclone centers at all given time steps and then in a second step all cyclones are tracked by connecting their identified locations in consecutive time steps. The more constraints are applied in the identification step, the narrower becomes the range and the number of the identified features. For example, in some studies the definition of the location of a cyclone implies three constraints on the fields of mean sea level pressure: (1) the representative grid point of the data field has to have the minimum value among the neighboring grid points; (2) the minimum value has to be inferior of a threshold value; and (3) the field gradient has to be superior of a threshold value (e.g. Murray and Simmonds, 1991; Blender and Schubert, 1997; Nissen et al, 2010). However, the application of "strict" constraints on pressure gradients may lead to tracking cyclones only close to their mature stage, whereas weak cyclones may not be detected at all.

A tracking algorithm needs to decide if the identified cyclones have moved over time or they have ceased to exist. In practice, this step is more complicated since cyclones can split or merge with other cyclones or there might exist more than one candidate to be considered for the next cyclone location. This is often the case in noisy fields, where an algorithm may identify a significant number of grid points located close to each other as cyclone centers. In this case, an algorithm has to determine which of the candidate features constitutes the next step of the tracked cyclone and which should be neglected. Many methods apply a “nearest neighborhood” approach where tracks are built by connecting the identified cyclone centers of a given time step with the nearest one of the following time step (Blender et al., 1997; Serreze et al., 1997; Trigo et al., 1999). Other studies use more complex tracking algorithms and utilize displacement speed (e.g. Murray and Simmonds, 1991; Wernli et al, 2006; Davis et al, 2008; Campins et al, 2011; Hanley and Caballero, 2012). These algorithms make a “guess” on the next step location of the cyclone and choose the nearest feature detected at that potential location. Finally, Inatsu (2009) presented an algorithm where tracking is based on neighbor enclosed area tracking, where cyclones are identified as areas of connected grid points that satisfy a certain condition; then tracking is performed by connecting the cyclone areas that overlap in consecutive time-steps.

Post-treatment of the tracked features has been proposed by Hodges (1999). His tracking algorithm constructs all tracks using the “nearest neighborhood” approach. Then, the tracks exchange track points until a cost function is minimized. The cost function is a measure of the smoothness of the total number of tracks. Hanley and Caballero (2012) also applied a post-treatment process in order to identify if cyclones, that present more than one center, undergo any merging or splitting process and adapt tracks accordingly.

Raible et al. (2008) were the first to compare the performance of three different tracking methods, applied on extra-tropical cyclones. Results converged on the interannual variability of cyclone occurrences; however they differed on the cyclone number trends and track densities. Recently the IMILAST project presented a comparison of the performance of 15 different algorithms which have been used for tracking extra-tropical cyclones during the cold season of 21 years over the entire planet (Neu et al, 2013). The tracks number, the cyclones life span and intensity may vary significantly depending on the algorithm. Indeed, there is a divergence on the algorithms results which is due to the fact that there is no common physical definition of a cyclone. Consequently, for each algorithm cyclone identification is performed by applying different constraints and/or different fields. In this sense, one of the main results of Neu et al. (2013) is that no algorithm is considered to be “superior” or more “correct” than the others, since cyclones are not defined in the same way. It is also noticeable that similar algorithms (in their configuration) might not present highly matching results. Despite the variety of the results, Ulbrich et al. (2013) showed that the algorithms have a common behavior when considering the extra-tropical cyclones tracks evolution in the context of a changing climate. This result confirms that independently of the different algorithms set-up and modeling constraints there is a common robust behavior.

In this study, our principal motivation is to design an algorithm which is able to provide qualitative characteristics of the tracked features, in parallel with the tracking (splitting, merging, wind speed, associated rainfall, minimum pressure etc.). A new aspect of the proposed approach is that cyclonic features are tracked based on their physical properties, by assuring a gradual evolution of the cyclone relative vorticity, and not on their displacement. The use of relative vorticity presents some advantages when compared to the use of geopotential height or mean sea level pressure: it is a high frequency variable, representative of local scales that -presumably- permits cyclone tracking since its initial perturbation and thus before it is characterized by closed pressure contours (Sinclair, 1994, 1997; Hodges 1999; Inatsu 2009; Kew et al, 2010). This can be an advantage when considering for instance explosive cyclogenesis where cyclones intensity increases significantly in twenty four hours (e.g. Sanders and Gyakum, 1980; Trigo et al, 2006; Lagouvardos et al, 2007). On the other hand, relative vorticity is a wind-based field, sensitive to the dataset horizontal resolution, while local maxima might not correspond to wind vortices but to other features such as an abrupt wind turning.

To deal with the spatial noise of relative vorticity, in our approach we smooth the input fields. The smoothing operation partly counteracts the advantage of relative vorticity to detect cyclones since their early stage, however our algorithm has a high degree of flexibility, that permits tracking of perturbations that did not evolve to strong cyclones. Similar setup has been also used in previous studies for capturing weak cyclonic features (e.g. Murray and Simmonds, 1991; Pinto et al, 2005), but in our approach this provides an added value for optimizing the algorithm and determining the cyclones that are not sensitive to filtering. The application and assessment of our method is done in line with the efforts of the IMILAST project, using the same time periods and input datasets, in order to make the results of our algorithm comparable with those of the aforementioned project.

In Section 2 the cyclone detection and tracking method is described in detail. In Section 3 we present the results of several sensitivity tests of our method, applied to the ERA-Interim (ERA-I) data set for the winters (December-January-February) of the period 1989-2009. Finally, Section 4 hosts the conclusions and our prospects.

2. Identification and tracking algorithm method

In this section we present our algorithm and its application on the vorticity fields at 850hPa level within the extra-tropical latitudes of the Northern hemisphere during the winters of 1989-2009. We use meteorological data from the 6-hourly ERA-I reanalyses with a horizontal resolution of 1.5°x1.5° (Uppala et al, 2008). The algorithm is composed by two independent steps: In the first step, the algorithm identifies all cyclonic features for all time steps of a dataset and in the second step it builds the cyclone tracks.

2.1 Step I: Identifying cyclones and quantifying their characteristics

The first step of the algorithm is devoted to the identification of the cyclones and to the quantification of their characteristics. First, the algorithm identifies all cyclonic features, or more precisely all cyclonic circulations. Then, for each cyclonic circulation the algorithm identifies all of its representative centers which will be treated as different cyclones. Finally, for each center, the algorithm quantifies its characteristics (e.g. maximum relative vorticity, maximum wind speed, minimum sea level pressure).

2.1.1 Identification of cyclonic circulations

To identify cyclonic circulations, the vorticity field is smoothed by applying a spatial filter. In previous studies a variety of filtering operations has been used to smooth the vorticity field such as bspline techniques (Hodges, 1995), time band-pass filtering (Hoskins and Hodges, 2002; Inatsu, 2009) and 1-2-1 filters (Satake et al, 2013). Here we use a simple method of a 1-1-1 spatial filter, which is however adequate to smooth out the orographic or coastal vorticity maxima as well as the gradients of relative vorticity fields. The latter helps the algorithm to reject local vorticity maxima that are nested within noisy field gradients, especially when considering very high resolution datasets. The smoothing operation on the relative vorticity field is performed at each grid point separately by multiplying the sum of all its neighboring X grid points by 1/(2X+1). For instance at any grid point a, b the smoothed Relative Vorticity (RV) is given by:

$$\frac{1}{2X+1}\cdot\sum_{i=a-X}^{a+X}\sum_{j=b-X}^{b+X}\left(RV_{a,b}\right) \qquad \text{Eq. 1}$$

As a result, the larger X is, the stronger is the smoothing operation on the relative vorticity field. Finally, we apply a threshold value and we retain only the grid points exceeding this threshold.

Figure 1 shows the raw relative vorticity fields and the filtered ones by applying three different filters with X equal to 3, 5 and 7. The relative vorticity fields are derived from ERA-I and they are centered over Europe at 00:00 UTC, 3 December 1999, featuring the Anatol storm over Denmark as the strongest detected cyclone. In all panels of Fig. 1 the threshold is set at 3×10^{-5} s^{-1}. The stronger the applied filter is, the weaker are the relative vorticity values. Small vorticity features tend to be suppressed but nevertheless, the structure and location of the vorticity maxima of the strongest features, as the Anatol storm, are not altered among the different filter operations. Filtering here is used for smoothing values within a cyclonic circulation. As a result, the filtering matrix should not be much larger than the length scale of a cyclone. In this sense, a 7x7 grid point filter for ERA-I means that relative vorticity is smoothed in a 10.5°x10.5° region which is certainly a large area.

As shown in Figs 1a and 1b, each cyclonic circulation might correspond to a unique cyclone or to a larger complex of cyclonic centers of more than one local maximum. The 3×10^{-5} s^{-1} threshold applied on the ERA-I dataset (1.5°x1.5° resolution) has been found adequate for describing cyclones even at their initial stage, for all three filtering sensitivity tests. In this step, the algorithm identifies and labels with a number all cyclonic circulations which are defined as the areas composed by neighboring grid points of values exceeding the $3x10^{-5}$ s^{-1} threshold. The selected threshold value is a good trade off for detecting cyclones in coarse resolution datasets (e.g. 1.5°x1.5°, as in ERA-I used here) and in high resolution datasets (e.g. 20km regional climate runs). A threshold may function conveniently as a constant for better adjusting the filtering strength. Alternatively, one could keep the filtering strength constant and make the threshold value vary. However, it is only by varying the filtering strength that the vorticity field may be smoothed within the characteristic length scale of cyclones. Similar approaches in identifying a feature through an enclosed area have been previously used for cyclones (e.g. Hodges 1999; Wernli et al, 2006; Inatsu, 2009; Flaounas et al 2013) as well as for other features such as MCS (e.g. Machado et al, 1998).

2.1.2 Identification of cyclonic centers

Inspection of Figure 1b, 1c and 1d reveals that not all cyclonic circulations correspond to a unique cyclone. For this reason each labeled cyclonic circulation is further treated in order to locate all embedded local vorticity maxima. These local maxima will be also labeled and eventually will be treated as centers of unique cyclones. The term “centers of unique cyclones” has no physical basis but it is conveniently used here in order to describe the grid points which present local maxima of relative vorticity and are followed in time in order to construct cyclones tracks. In this sense we need to provide the algorithm with a representative cyclone center even though the cyclone structure might be very complex with more than one vorticity maximum, especially in very high resolution datasets. To deal with this issue, (1) we filter the data, smoothing the noisy gradients (already performed in the previous step), (2) we define the local maximum as the maximum value of the central grid point among its eight surrounding grid points and (3) we consider that between two centers there is a relative vorticity difference greater than a threshold value (in this case set equal to $3x10^{-5}$ s^{-1}) which is applied to define the cyclonic circulations. The last criterion prohibits weak cyclonic circulations (i.e. identified cyclones of relative vorticity close to the threshold value) to present multiple centers.

2.1.3 Quantifying cyclone characteristics

Once all cyclones have been identified, we determine an "effective area" for each cyclone. This area is a circular disk centered at the cyclone vorticity maximum, as identified in the previous step. The disk radius grows gradually until: (1) all grid points included in the disk have a vorticity average inferior to a threshold value, or (2) until the radius reaches a pre-defined maximum length, or (3) until a relative vorticity value greater than that of the cyclonic center, is found within the area. According to this empirical method, strong or large and weak cyclones tend to produce large effective areas. The third criterion favors the stronger cyclones to spread their area independently of the presence of other weaker ones in their region, while it restrains the weaker cyclones to share the same area with stronger cyclones. In Flaounas et al. (2013) the cyclone area was defined by the cyclone enclosed contour as defined by the applied threshold value (see their appendix figure). However, such an enclosed area might not capture grid points that present relative vorticity values lower than the applied threshold. In Lim and Simmonds (2007) the cyclone area was defined by a representative circular disk of a radius defined equal with the average distance between the cyclone center and the enclosing zero contour of the mean sea level pressure laplacian. In our algorithm the circular disk seemed the best choice in order to capture the areas affected by a cyclonic vortex, although more "irregular shapes" might be considered, as for instance enclosed contours of pressure (Wernli et al, 2006; Hanley and Caballero, 2012) or of relative vorticity (Flaounas et al, 2013).

Once the effective area is defined, our algorithm computes the physical properties of the cyclone within it. As an example, Fig. 2 shows the effective area and the detected minimum sea level pressure and maximum 10-meter wind of the storm Anatol at the same time as in Figure 1b.

2.2 Step II: Tracking cyclones

Before combining the cyclone centers into a track, the algorithm sorts the identified cyclones based on their relative vorticity value, from the strongest (i.e. the one with the highest relative vorticity value) to the weakest. Then, it starts from the first cyclone and searches forward and backward in time for all its possible tracks. More precisely, the algorithm constructs all possible cyclone tracks which present the same highest vorticity state. Once all possible tracks are constructed, the algorithm chooses the track that presents the most "natural evolution" of relative vorticity, i.e. the track which presents the smallest differences of relative vorticity in consecutive points, weighted by the distance between the track point locations.

Figure 3a illustrates an idealized experiment, presenting the locations of all identified cyclones in a four time step dataset. Six cyclones are identified: one cyclone in the first time step, one cyclone in the second time step and two cyclones for each of the time steps three and four. The tracking process begins from the strongest cyclone (i.e., the cyclone 2(12)) and constructs all possible tracks by iterating forward and backward in time with all other features. Figure 3b shows that the first cyclone may undertake four possible tracks, however it is obvious that the track 1(9), 2(12), 3(10), 4(8) presents the most "natural evolution", since maximum relative vorticity presents the smallest difference from one time step to the next. The algorithm saves this track and deletes the used cyclones' locations from the dataset. Then, a new iteration begins where the algorithm will start from the cyclone with the highest vorticity and eventually a new track will be constructed (Figure 3c). Starting the tracks from the cyclone's mature state was found to be more efficient for the first steps of the tracks construction. Indeed, in the previous and next time step of the cyclone with the highest vorticity state, for most cases, there is only one strong cyclone to act as a candidate for continuing the tracks.

The practice of cost function minimization has been used in relevant literature on tracking algorithms. . Namely, Hodges (1995) builds the feature tracks by minimizing the cost function of the feature's track smoothness while Hewson and Titley (2010) by applying likelihood score on the feature's physical characteristics. Here, the feature's evolution in each track is determined by a cost function (C), represented by the absolute average difference of the relative vorticity weighted by the distance between two consecutive time steps:

$$C = \frac{\sum_{n=1}^{n=N-1} d_{n\to n+1}(|V_{n+1} - V_n|)}{\sum_{n=1}^{n=N-1} d_{n\to n+1}} \qquad \text{Eq. 2}$$

Where $\boldsymbol{C}$ is the cost function of a candidate track, $\boldsymbol{N}$ is the total number of the track's time steps, $\boldsymbol{d}$ is the distance between two consecutive track points and $\boldsymbol{V}$ is the relative vorticity at each time step.

The number of possible tracks is quite large. However, their number can be significantly reduced by the application of a series of legitimate heuristics, that remove those tracks that present a non-natural behavior: (1) from each time step to the next, the location of the next candidate cyclone must be within a threshold range, (2) the maximum vorticity between the tracked cyclone and a candidate cyclone must not differ more than 50% and (3) if the displacement is more than 3° long between two successive displacements, then the angle between these displacements must be greater than 90°. The first constraint prohibits the algorithm from searching for next step candidate features in locations where the tracked cyclone could by no means be displaced. In our algorithm the cyclones are searched within a 5°x10° latitude-longitude range which is the largest possible displacement for extratropical cyclones as proposed by Hodges (1999). The second constraint prohibits the algorithm from choosing candidates which consist by no means a possible evolution of the tracked feature. The use of a percentage is highly convenient since large vorticity values are subject to higher changes between consecutive time steps compared to small vorticity values. Finally, the third constraint prohibits the algorithm to take into account abrupt backs-and-forths of the cyclone's movement. Such displacements are more likely to take place in raw vorticity fields, where local maxima might change abruptly. For instance the algorithm would not choose the track 2(12), 3(4) and 4(8) in Figure 3 since the consecutive displacements present an angle of 74° (marked in red in Fig. 3) which is smaller than 90°.

Finally, our algorithm returns as output for each track a matrix that contains information on the cyclone's track and physical characteristics. The matrix has a number of rows which is equal to the track points and a number of columns equal to the algorithm standard outputs plus the number of physical diagnostics. The optional output diagnostics might vary depending on the study needs and the data inputs. Labeling the cyclonic circulations (section 2.1.1) and the cyclonic centers (section 2.1.2) within the tracks permits a post-treatment analysis for determining merging and splitting of cyclones. For our application on the extra-tropical cyclones only maximum 10-meter wind speed and sea level pressure minima are considered. As an example of the algorithm performance, Fig. 4 presents two cyclone tracks which evolve by sharing the same cyclonic circulation. The tracks are supported by the physical characteristics of the cyclones (evolution of relative vorticity, maximum 10-meter wind speed and minima of sea level pressure), demonstrated in Figure 5.

It is likely that our method detects fronts associated with vorticity maxima as cyclone centers, especially when applied to high resolution datasets (e.g. regional climatic simulations). In order to avoid the detection of a frontal zone, additional criteria of high or low complexity should be considered (e.g. Hewson and Titley, 2010). However, such criteria could be dependent on several factors -as for instance the spatial resolution of the dataset- and would result to a "stricter" cyclone definition. The more precise the mathematical criteria, the more constrained are the tracking results to systems of specific characteristics. In the case of fronts, the latter could for instance exclude the early stages of certain tracked cyclones that emerge from high vorticity frontal areas of a "parent" cyclone.

An example of a front detection is illustrated in the two cyclones cases, presented in Fig. 4. Inspection of surface pressure charts (not shown) showed that the first track point of the second cyclone (red dot in Fig. 4b) corresponds to the front of an extra-tropical cyclone (the one depicted by the black track). In the following time steps (Fig 4c to 4f), this secondary vorticity maximum evolves to a strong cyclone (red track) which presents its own low pressure minimum. Here we capture the initial stage of the vorticity maximum, before the occurrence of a pressure minimum. Nevertheless, not applying additional criteria might demand post-treatment of the track results in order to exclude "wrong" tracks or tracks that do not match the research needs.

3. Application the tracking algorithm in a climatological context and sensitivity in different parameters

In this section we present the results of the application of the algorithm for all winters (December, January and February) of the period 1989-2009 along with the results of three sets of sensitivity tests:(a) on relative vorticity filtering, (b) on the cost function of Eq. 2, and (c) on the constraint that relative vorticity between two consecutive track points must not differ more than 50%. In all sensitivity tests, the threshold used to define cyclones is $3x10^{-5}$ s^{-1} and we analyze only tracks with a life time of at least one day.

3.1 Method sensitivity on filtering the relative vorticity field

In this section we apply three different filter strengths (described in section 2.1.1) to the ERA-I dataset. The applied spatial filters correspond to a 3x3, a 5x5 and a 7x7 grid points filtering, named as *filter3*, *filter5* and *filter7*, respectively. Figure 6a presents the number of detected cyclonic centers as a function of their relative vorticity for all three sensitivity tests and Fig. 6b their relative frequency. Since all tests are bounded to identify cyclones exceeding a common threshold of $3x10^{-5}$ s^{-1} and since filtering decreases the relative vorticity values, due to its smoothing operation, it is of no surprise that the total number of detected cyclone centers is reduced with increasing filtering intensity. Regardless the spatial filtering strength, all three sensitivity tests present a logarithmic distribution (Fig. 6a), while the stronger the filter the more cyclones intensities are reduced (Fig. 6b).

Strong filtering versus weak filtering may have two effects: first it tends to detect fewer tracks, which also correspond to the stronger cyclones, and second it tends to reduce the cyclone track lengths (by not taking into account the weakest vorticity perturbations in the early and late stages of a cyclone track). The validity of the first hypothesis is evident from Fig. 1 where smoothing suppresses many weak cyclonic centers, but stronger cyclones (such as the Anatol storm) are equally detected with all three filters. To verify the second hypothesis we investigate the characteristics of the tracks as detected by *filter3*, *filter5* and *filter7*. Figures 7a, 7b and 7c show the distribution of the relative frequency for the life-time of cyclone tracks, the average speed of the cyclones and their maximum relative vorticity. No significant changes between the results obtained with the different filters are observed when considering the cyclone life-time. Consequently, the second hypothesis that average track characteristics are sensitive to filtering can be rejected. It is interesting though that our applications using weak filtering detect weak cyclones that have similar life scales. The fact that the distributions of the relative frequencies of the average speed of cyclones in Fig. 7b is also similar for all three filters means that the weaker cyclones in *filter3* and *filter5* do not correspond to weak stationary vorticity perturbations, but nevertheless they also do not evolve to strong extra-tropical cyclones. The dynamical reasons for not evolving to strong cyclones are an interesting issue; however, it is out of the scope of this paper.

In order to verify the cyclone tracks location, Fig. 8 shows the Cyclones Center Density (CCD) for all three filtering strengths. It is evident that different magnitudes of CCD are observed, depending on the filtering strength, however, the spatial pattern remains coherent for all three cases. A question that may arise is whether weak cyclones in the strongly filtered sensitivity tests correspond to strong cyclones in the weakly filtering tests. To address this question we took into account all points of the distributions in Fig. 6 and we associated the common points between *filter3* and *filter7* (points sharing the same timing and having a distance inferior of 5°). Results showed that *filter7* shared 52% of its points (2331 points) with *filter3*. The median of the intensity of the common points of *filter3* corresponded to the 78th percentile of all *filter3* points' intensity. Consequently cyclones in *filter7* correspond to the strongest cyclones of the weakly filtered datas. This comes in accordance with the relative frequency of cyclone centers intensity in Fig. 6b, where most of *filter7* identified cyclones are concentrated to weaker relative vorticity values, respect to *filter3* and *filter5*.

The effect of filtering (for instance *filter7* compared to *filter3*) is characteristic to the CCD within the Mediterranean region, where the cyclones are known to be weaker (Campa and Wernli, 2012) than the other extratropical cyclones forming over the oceans. Indeed, in *filter7* there is a dramatic decrease of detected cyclones over the Mediterranean Sea, compared to *filter3* and *filter5*. Figure 8 presents a high similarity with the results from other algorithms (Neu et al., 2013) independently if filtering is performed or if sea level pressure or relative vorticity is used as input for the detection of cyclones. Indeed CCD maxima are distinctly located over the Pacific Ocean, the Northern Atlantic Ocean, and the Mediterranean. Furthermore, regardless the filtering strength, both cyclone speed and life time relative frequency distributions (Figs. 7a and 7b) seem to be in good agreement with the other algorithms (Neu et al, 2013) presenting most probable cyclone speeds between 30 to 40 km/hour and cyclone life time relative frequency distributions decreasing exponentially from less than 2 days up to a total of approximately 8 days.

Figure 9 presents the time series of the number of cyclone centers. For all three filters, our results are in agreement with those of Neu et al. (2013) showing no specific inter-annual trend. As expected, the cyclone center number per year depends on the filtering strength. The cyclone center numbers decrease from approximately 9000/year for *filter3* to approximately 3000/year for *filter7*. All three tests are within the ranges of other algorithms which range from 2000/year to 12000/year but it is only *filter5* which is consistent with the majority of other algorithm results which calculated 4000 to 7000 cyclonic centers per year. The time series phasings are in good agreement between *filter3* and *filter5*, presenting a correlation score of 0.91. On the other hand, the correlation score between *filter5* and *filter7* is 0.43, suggesting that the time series phasing between the two sensitivity tests is dependent to the weaker cyclones that are suppressed in filter7. This should not raise a question on the “correctness” of the different test results, but rather on the results independence to the different filtering strengths.

3.2 Method sensitivity on tracking parameters

As already mentioned, two additional sets of sensitivity tests have been performed in order to test the tracking method (step II) results. The first set of the sensitivity experiments relates with the cost function (Eq. 2) and it is composed by the following members: (a) S_{rel}, where the final track choice is only dependent to the track relative vorticity evolution (Eq. 3) and (b) S_{dist}, where the cost function is only dependent to the distance between consecutive track points (Eq. 4).

$$C = \sum_{n=1}^{n=N-1} (|V_{n+1} - V_n|) \quad \text{Eq. 3}$$

$$C = \sum_{n=1}^{n=N-1} d_{n \to n+1} \quad \text{Eq. 4}$$

The second set relates with the constraint that the relative vorticity between consecutive track points may not vary by more than 50% (Section 2.2) and it is composed by three members, where the 50% threshold has been modified to 25% ($S_{25\%}$), 75% ($S_{75\%}$), 100% ($S_{100\%}$), while the original cost function

(Eq. 2) has been used. For both sets we used the identified cyclones from *filter3* since this is the dataset with the highest number of identified cyclones (Fig. 6), amplifying the differences between the tracking results of the sensitivity tests.

Figure 10 presents the tracks life time and average speed for both sets of sensitivity experiments. The results of the first set of experiments that focus on the cost function (Figs 10a and 10b), show that the cyclones life time and average speed is quasi-equal for all *filter3*, S_{rel} and S_{dist} (maximum differences are less than 1%). This suggests that the number of track points (i.e. life time) and distance between the track points (i.e. average speed) are rather insensitive to the change of the cost function. This is due to the fact that the algorithm always presented several alternative tracks for a single cyclone but in the majority of the cases, these alternative tracks were similar and only presented short deviations from the cyclones' main path. In such cases, the usefulness of the cost function is on choosing the smoothest track in terms of intensity and distance between consecutive track points. It is noteworthy that in S_{rel} and S_{dist}, the algorithm was still bounded by the constraint of linking cyclone centers that presented relative vorticity values that did not vary by more than 50%. Climatologically, the term ***d*** in the cost function does not add significantly to the performance of the algorithm. However, for certain cases it seemed useful to weight the vorticity differences by the distance, especially when the candidate cyclones presented similar vorticity with the tracked cyclone, but were located unrealistically far from it.

The results of the second set of experiments that relate with the 50% threshold (Figures 10c and 10d) reveal similar distributions for all varying thresholds, however when comparing $S_{100\%}$ and $S_{25\%}$, the former tends to form longer tracks (Fig. 10c) with longer distances between the track points (Fig. 10d). Indeed, when applying stricter (loose) thresholds on the permitted evolution of the cyclones intensity, then it is more likely that the algorithm will form shorter (longer) tracks due to the smaller (larger) accepted differences on the relative vorticity evolution of consecutive track points. Ideally, the 50% threshold could be neglected; however this would create numerous alternative tracks when the input datasets are of high resolution. In general, the constraints applied in step II (i.e. 50% threshold, searching cyclones within a 10°x5° area and the angle criterion; Section 2.2) have been found as a fair compromise between cutting off “unnatural” possible cyclone tracks and providing all possible tracks for the algorithm to depict the “correct” one according to the cost function.

3.4 Physical coherence of the tracked cyclones

In this section we perform an analysis of the effective area diagnostic tool (described in section 2.1.3) by retaining only the cyclone tracks of *filter3* after calibrating its results (i.e. taking into account the dashed lines of *filter3* in Fig. 9). Figure 11 presents the composite life cycle of the cyclones physical characteristics, centered on the time of the maximum vorticity of the tracks (mature stage) and averaged for all tracks detected in the Pacific Ocean (from 130° to 240° of longitude and from 30° to 90° of latitude), North Atlantic Ocean (from 300° to 360° of longitude and from 30° to 90° of latitude) and within the Mediterranean region (from 345° to 45° of longitude and from 25° to 50° of latitude). The results show that regardless of the region, there is a strong coherence between the life cycle of sea level pressure minima, relative vorticity and maximum 10-meter wind speed. The strength of the cyclones tends to increase rapidly but decays with a slower rate. This slow weakening of the cyclones' intensity in the composite time series of Fig. 11 is due to the fact that the duration of the cyclones mature stage is highly variable (as shown in Fig. 7). Here, for the construction of the composites there is no distinction on the cyclones life time, while one should note that the further we get from the time of the cyclone maximum vorticity (i.e. the composite center) the fewer cyclones last long enough to provide diagnostics for the composites. For instance, the Mediterranean cyclones life-time scale is inferior from the other extra-tropical cyclones and rarely exceeds 2-3 days. Nevertheless, our motivation here is to assess the validity of the effective area diagnostic which seems to capture correctly the life cycle of cyclones physical characteristics regardless the region. Indeed, in agreement with Campa and Wernli (2012), Mediterranean cyclones are less deep, in terms of sea level pressure, while Atlantic cyclones are slightly deeper than those occurring over the Pacific Ocean.

4. Conclusions

In this article we presented a new algorithm for identifying and tracking cyclones, applied on winter extra-tropical cyclonic systems over the northern hemisphere. The algorithm performance was tested for three different strengths of filtering applied on the high frequency relative vorticity fields. The results showed that the number of tracks were inversely proportional to the filter strength while the cyclone spatial and temporal variability was coherent with those produced by other tracking algorithms presented in the literature. Finally, the algorithm was shown to successfully capture the physical characteristics of cyclones.

As in previous methods in literature, our identification and tracking algorithm for cyclones uses the fewer constraints possible, not only for tracking weak vorticity perturbations which evolved in strong cyclones, but also for tracking weak perturbations that did not evolve into strong cyclones. This permits the better calibration of the algorithm, but also in a future work the more precise description of the environmental conditions which favor cyclogenesis and cyclone intensification. Furthermore, we chose the vorticity criteria to vary dynamically (vorticity must not vary more than 50% in consecutive time steps) and we avoided any threshold or cut-off values which would prohibit tracking cyclones of “anomalous behavior”. It should be noted that although in this study we applied the algorithm based on relative vorticity to identify and track cyclones, the same algorithm might be applied on any dataset which presents enclosed areas after applying a threshold value. For instance the algorithm could be applied on datasets of brightness temperature or cloud cover for tracking supercells or mesoscale convective systems.

Tracking uses a cost function minimization approach, based on the cyclone relative vorticity maxima. Mistakes were observed especially when cyclonic circulations were found to be very noisy with multiple local maxima. As an alternative to the vorticity-based cost function used here, it would be interesting to use the weighted mean differences of additional cyclone physical characteristics (pressure, wind speed etc.) between consecutive time steps. This has been previously applied by Machado et al. (1998) for tracking MCS based on brightness temperature satellite observations. However, their method assumes a-priori choice of the weighting value, risking restraining our method adaptability to track cyclones of different origin (e.g. extra-tropical and tropical cyclones). Our algorithm links cyclone centers in consecutive time steps, in contrast with the alternative configuration proposed by Machado et al (1998) and Inatsu (2009) to link enclosed areas. This decision was made because if enclosed areas were linked, then large cyclonic circulations would not correspond to a single cyclone and additional criteria -and/or filtering- would be needed, while weak cyclones would be neglected.

Further development of the algorithm includes (1) extension of the identification part in three dimensions and (2) extension of the method adaptability for different atmospheric features such as MCS. The algorithm source is freely available in MatLab language upon request to the corresponding author.

Acknowledgements

EF was supported by the IMPACT2C program (funded by the European Union Seventh Framework Programme, FP7/2007- 2013 under the grant agreement 282746) and this work has been conducted in the Institut Pierre Simon Laplace group for regional climate and environment studies. The authors are grateful to Philippe Drobinski and Heini Wernli for fruitful discussions on the algorithm configuration, and to Christoph Raible for his help in plotting the cyclone centers density field.

References

Allen, J.T., Pezza, A.B., and Black, M.T.: Explosive cyclogenesis: a global climatology comparing multiple reanalyses, J. Climate, 23, doi: 10.1175/2010JCLI3437.1, 2010.

Blender, R., Fraedrich, K., and Lunkeit, F.: Identification of cyclone-track regimes in the north atlantic., *Quart. J. Royal Meteor. Soc.*, 123, doi: 10.1002/qj.49712353910, 1997.

Blender, R., and Schubert, M.: Cyclone Tracking in Different Spatial and Temporal Resolutions, *Mon. Wea. Rev.*, 128, 377–384, 2000.

Čampa, J., and Wernli, H.: A PV Perspective on the Vertical Structure of Mature Midlatitude Cyclones in the Northern Hemisphere, *J. Atmos. Sci.*, **69**, DOI: 10.1175/JAS-D-11-050.1 , 2012.

Campins, J., Genoves, A., Picornell, M.A., and Jansa, A.: Climatology of Mediterranean cyclones using the ERA-40 dataset, *Int. J. Climatol*, 31, doi:10.1002/joc.2183, 2011.

Davis, C.A., Snyder, C., and Didlake, A.: A vortex-based perspective of eastern Pacific tropical cyclone formation, *Mon. Wea. Rev.*, 136, DOI: 10.1175/2007MWR2317.1, 2008

Eckhardt, S., Stohl, A., Wernli, H., James, P., Forster, C., and Spichtinger, N.: A 15-Year Climatology of Warm Conveyor Belts, *J. Climate*, 17, 218–237, 2004.

Flaounas, E., Janicot, S., Bastin, S., Roca, R., and Mohino, E.: The role of the Indian monsoon onset in the West African monsoon onset: observations and AGCM nudged simulations, *Climate Dynamics*, 38, doi: 10.1007/s00382-011-1045-x, 2012.

Flaounas, E., Drobinski, P., and Bastin, S.: Dynamical dowscaling of IPSL-CM5 CMIP5 historical simulations over the Mediterranean: Benefits on the representation of regional surface winds and cyclogenesis, *Clim. Dyn.*, doi: 10.1007/s00382-012-1606-7, 2013.

Hanley, J., and Caballero, R.: Objective identification and tracking of multicentre cyclones in the ERA-Interim reanalysis dataset, *Q. J. R. Meteorol. Soc*., 138, doi:10.1002/qj.948, 2012.

Hewson, T.D., and Titley, H.A.: Objective identification, typing and tracking of the complete life-cycles of cyclonic features at high spatial resolution. Met. Apps, 17: 355–381, 2010

Hodges, K.I.: A general method for tracking analysis and its application to meteorological data, Mon Wea Rev, 122, 2573–2586, 1994

Hodges, K.I.: Feature tracking on the unit sphere, Mon Wea Rev, 123, 3458–3465, 1995.

Hodges, K.I., Adaptive constraints for feature tracking, *Mon. Wea. Rev.*, 127, 1362–1373, 1999.

Hoskins, B.J., and Hodges, K.I.: New perspectives on the Northern Hemisphere winter storm tracks, *Journal of Atmospheric Science* 59, 1041–1061, 2002.

Inatsu, M.: The neighbor enclosed area tracking algorithm for extratropical wintertime cyclones. *Atmosph. Sci. Lett.*, 10, doi: 10.1002/asl.238, 2009.

Kew, S.F., Sprenger M., and Davies H.C, Potential vorticity anomalies of the lowermost stratosphere: A 10-yr winter climatology, *Mon. Wea. Rev.*, **138**, 1234–1249, 2010.

Lagouvardos, K., Kotroni, V., and Defer E.: The 21-22 January 2004 explosive cyclogenesis over the Aegean Sea: observations and model analysis, *Quarterly Journal of Royal Meteorological Society*, 133, doi: 10.1002/qj.121, 2007.

Lim, E.P., and Simmonds, I.: Southern Hemisphere Winter Extratropical Cyclone Characteristics and Vertical Organization Observed with the ERA-40 Data in 1979–2001, *J. Climate*, **20**, 2675–2690, 2007.

Limbach S., Schömer E., and Wernli H., Detection, tracking and event localization of jet stream features in 4-D atmospheric data, Geosci. Model Dev., 5, 457-470, 2012

Machado, L.A.T., Rossow, W.B., Guedes, R.L., and Walker, A.W.: Life Cycle Variations of Mesoscale Convective Systems over the Americas, *Mon. Wea. Rev*, 126, 1630–1654, 1998.

Murray, R.J., and Simmonds, I.: A numerical scheme for tracking cyclone centres from digital data. Part I: Development and operation of the scheme, Austr. Meteorol. Mag, 39, 155–166, 1991.

Neu, U., and Coauthors: IMILAST: A Community Effort to Intercompare Extratropical Cyclone Detection and Tracking Algorithms, *Bull. Amer. Meteor. Soc.*, **94**, 529–547, 2013.

Nissen, K.M., Leckebusch, G.C., Pinto, J.G., Renggli, D., Ulbrich, S., and Ulbrich, U.: Cyclones causing wind storms in the Mediterranean: Characteristics, trends and links to large-scale patterns, *Nat. Hazards Earth Syst. Sci.*, 10, doi:10.5194/nhess-10-1379-2010, 2010.

Pinto, J.G., Spangehl, T., Ulbrich, U., and Speth, P.: Sensitivities of a cyclone detection and tracking algorithm: individual tracks and climatology, Meteorol Z, 14, 823–838, 2005.

Raible, C.C., Della-Marta, P.M., Schwierz, C., Wernli, H., and Blender, R.,: Northern Hemisphere Extratropical Cyclones: A Comparison of Detection and Tracking Methods and Different Reanalyses. *Mon. Wea. Rev.*, **136**, 880–897, 2008

Roca, R., Lafore, J.P., Piriou, C., and Redelsperger, J.L.: Extratropical Dry-Air Intrusions into the West African Monsoon Midtroposphere: An Important Factor for the Convective Activity over the Sahel, *J. Atmos. Sci*, 62, 390–407, 2005.

Sanders, F., and Gyakum, J.R.: Synoptic-dynamic climatology of the 'bomb', *Mon. Wea. Rev.*, **108,** 1589–1606, 1980.

Satake, Y., Inatsu, M., Mori, M., Hasegawa, A.: Tropical Cyclone Tracking Using a Neighbor Enclosed Area Tracking Algorithm. *Mon. Wea. Rev.*, 141, 3539–3555, 2013

Serreze M., Carse, F., Barry, R., and Rogers, J.: Icelandic low cyclone activity: climatological features, linkages with the NAO, and relationships with recent changes in the Northern Hemisphere circulation, Journal of Climate, 10(3), 453–464, 1997.

Sinclair, M.R.: An Objective Cyclone Climatology for the Southern Hemisphere. *Mon. Wea. Rev.*, **122**, 2239–2256, 1994

Sinclair, M.R.: Objective Identification of Cyclones and Their Circulation Intensity, and Climatology. *Wea. Forecasting*, **12**, 595–612, 1997

Trigo, I., Davies, T., and Bigg, G.: Objective climatology of cyclones in the Mediterranean region, Journal of Climate 12(6): 1685–1696, 1999.

Trigo, I.F.: Climatology and interannual variability of stormtracks in the Euro-Atlantic sector: a comparison between ERA-40 and NCEP/NCAR reanalyses, Clim Dyn, 26, 127–143, 2006.

Wernli, H., and Schwierz, C.: Surface cyclones in the ERA-40 dataset, part I, novel identification method and flobal climatology, J Atmos Sci, 63:2486–2507, 2006.

Wernli, H., and Sprenger, M.: Identification and ERA-15 climatology of potential vorticity streamers and cutoffs near the extratropical tropopause, *J. Atmos. Sci.*, 64, 1569–1586, 2007.

Ulbrich, U., Leckebusch, G.C., and Pinto, J.G.: Extra-tropical cyclones in the present and future climate: a review, *Theoretical and Applied Climatology.*, 96, doi: 10.1007/s00704-008-0083-8, 2009.

Ulbrich, U. and co-authors: Are Greenhouse Gas signals of Northern Hemisphere winter extra-tropical cyclone activity dependent on the identification and tracking methodology?, Meteorol Z, 22, doi:10.1127/0941-2948/2013/0420, 2013.

Uppala, S., Dee D., Kobayashi, S., Berrisford, P., and Simmons, A.: Towards a climate data assimilation system: status update of ERA-interim, ECMWF Newsletter, 115, 12–18, 2008.

Figure captions

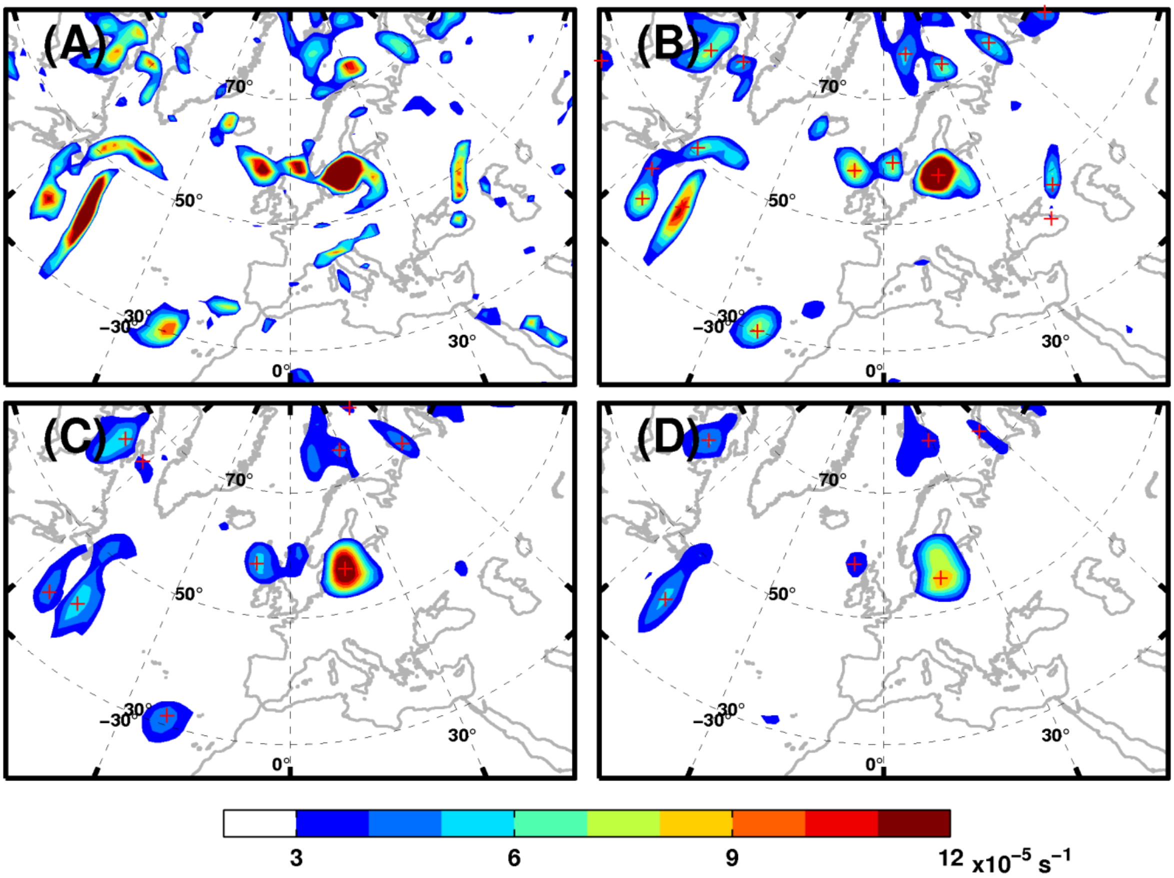

Figure 1 A) Relative vorticity raw fields at 00:00 UTC, 3 December 1999. The threshold applied is $3x10^{-5}$ s^{-1}. Crosses represent the central maxima located in the center of a 3x3 grid point area. B) as in (A) but relative vorticity field is filtered using a 3x3 correlation spatial filter. C) as in (A) but relative vorticity field is filtered using a 5x5 correlation spatial filter. D) as in (A) but relative vorticity field is filtered using a 7x7 correlation spatial filter.

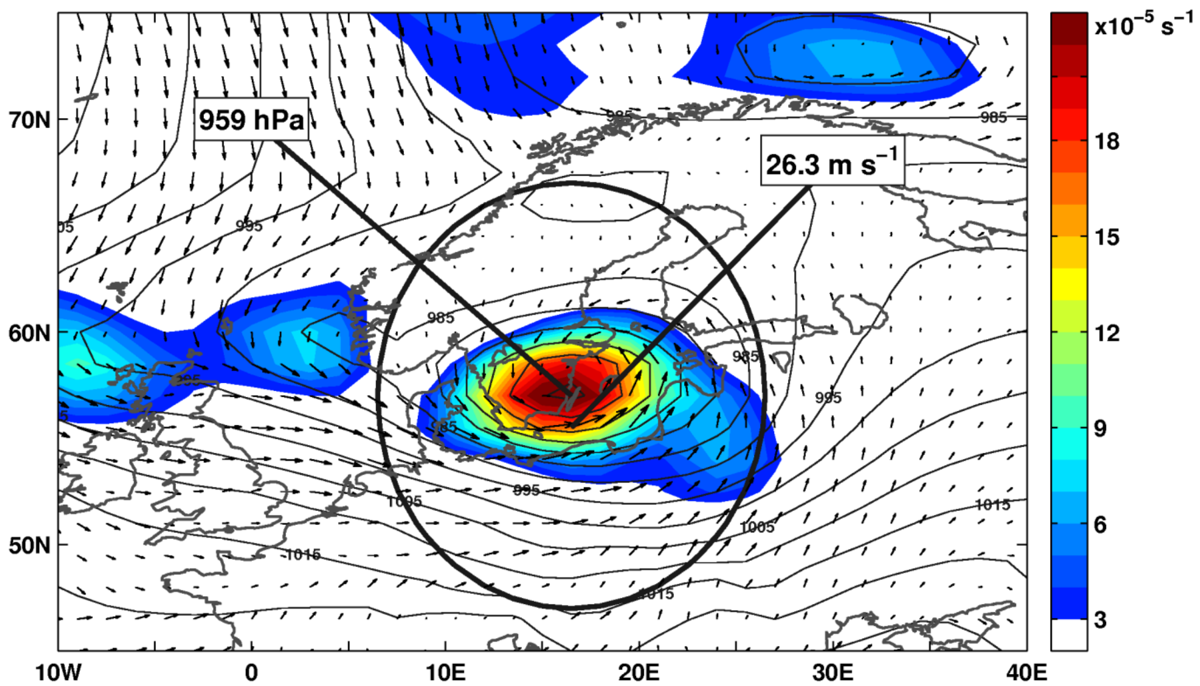

Figure 2 The Anatol storm at 00:00 UTC, 3 December 1999. Relative vorticity smoothed by a 3x3 spatial filtering (*color*), mean sea level pressure (*in contour*) and 10-meter wind field (*in arrows*). Thick black contour represents the cyclone effective area. Locations and values of maximum wind speed and lower pressure is depicted by the thick lines.

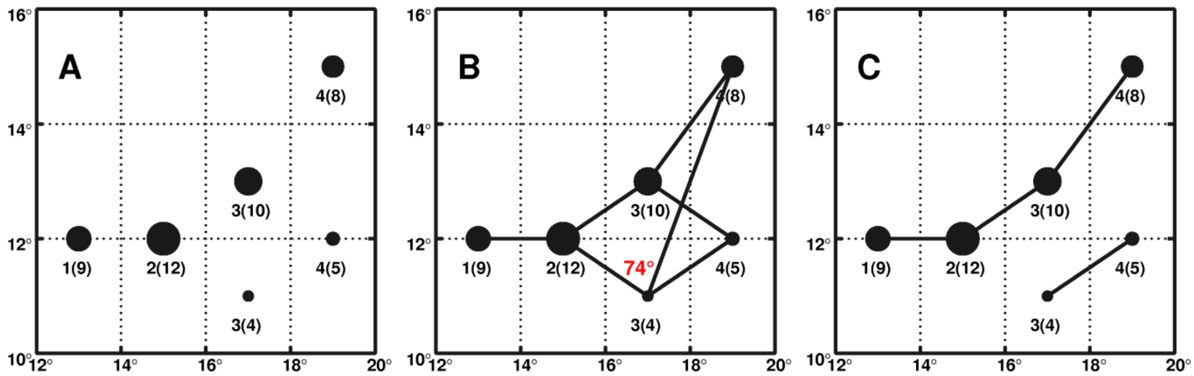

Figure 3 A) An idealized case of cyclone locations in four time steps. Locations are depicted by *circles*. Numbers above the locations are in the form X(Y), where *X* denotes the time step and *Y* the relative vorticity. Circles size is proportional to the cyclones relative vorticity value. B) all possible trajectories of cyclone 2(12) searching backwards and forward in time. C) Track results after retaining in B the track which presents the minimum average change of relative vorticity in successive time steps.

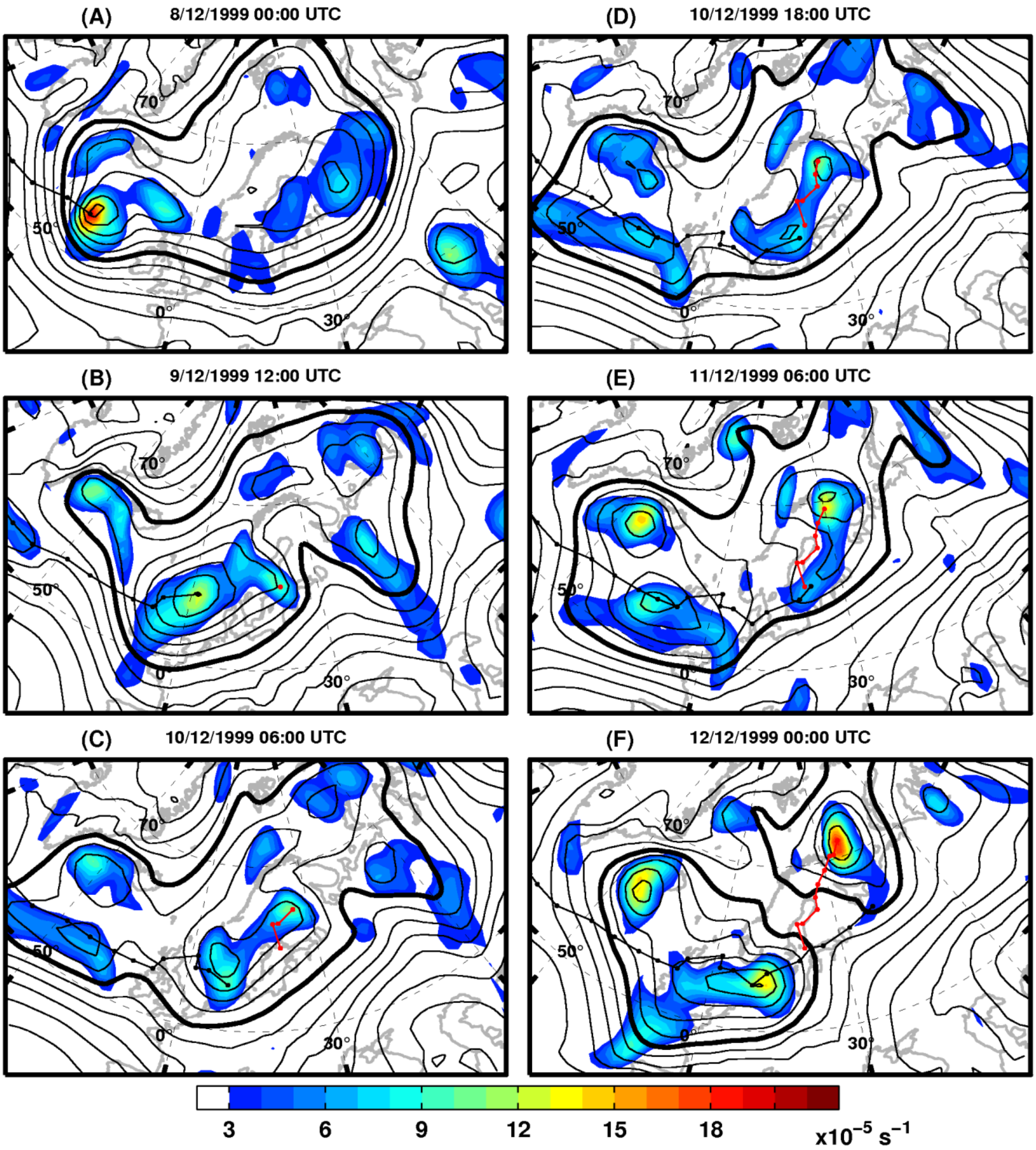

Figure 4 Relative vorticity smoothed by a 3x3 spatial filter (*color*), sea level pressure (*contours*, with a 5 hPa interval, thick contour denotes 1000hPa) and tracks (thin lines) of two splitting cyclones for different time frames in December 1999.

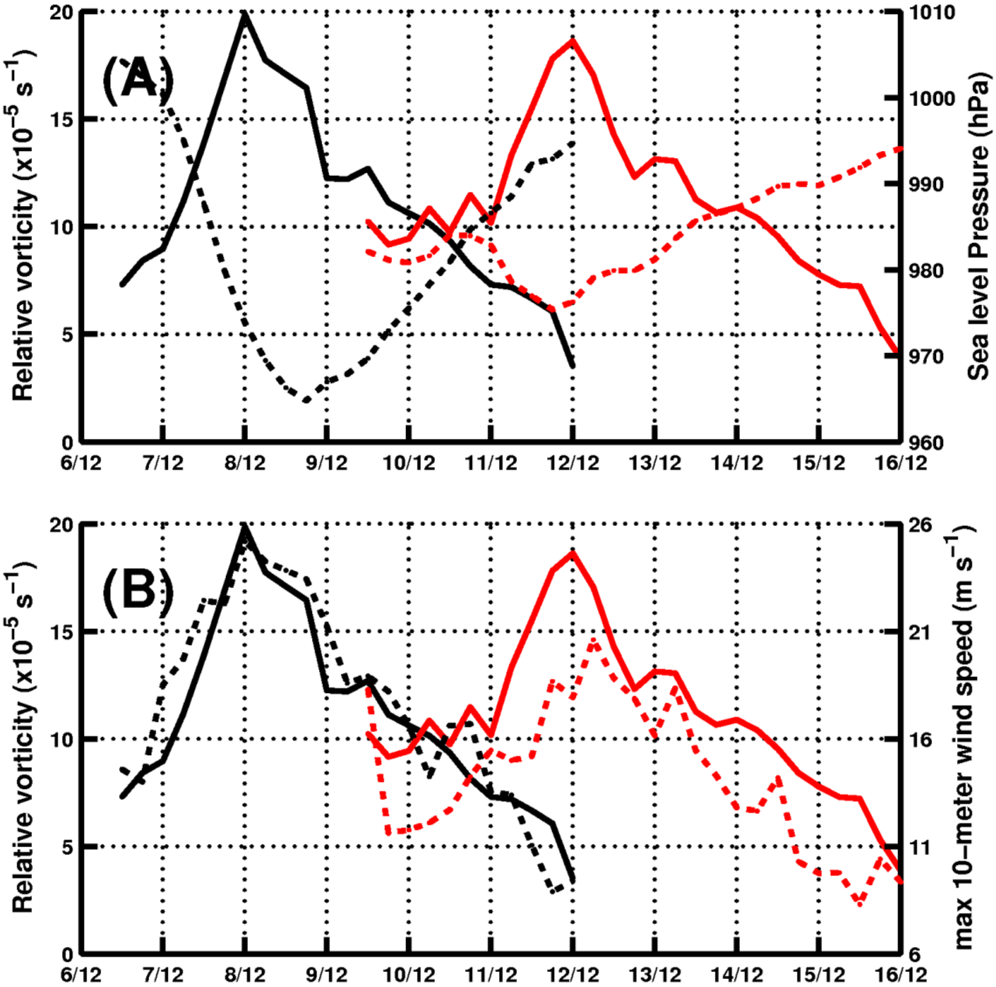

Figure 5 (A) Maximum relative vorticity (solid line) at the track centers and minimum sea level pressure (dashed line) as detected within the cyclones effective area for the two cyclones shown in Fig. 4 (B) as in (A) but dashed line corresponds to maximum 10-meter wind speed. Color lines are the same as in the tracks in Fig. 4. The horizontal axes represent the period 6-16 December 1999.

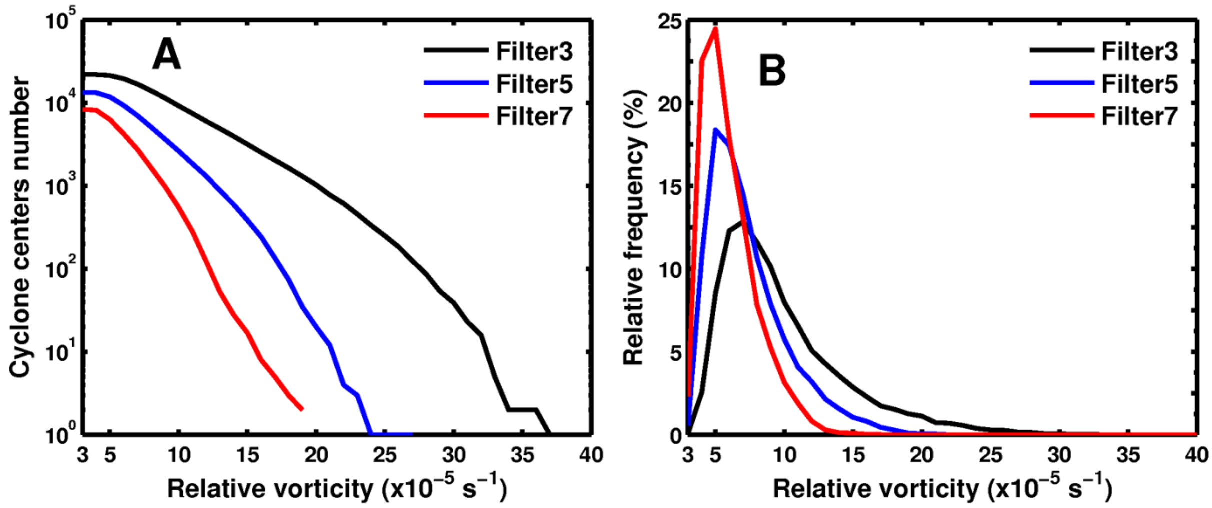

Figure 6 Number of cyclonic centers in function of their relative vorticity, as detected in the three algorithm sensitivity tests. B) Relative frequency distributions of the relative vorticity for the identified cyclone centers.

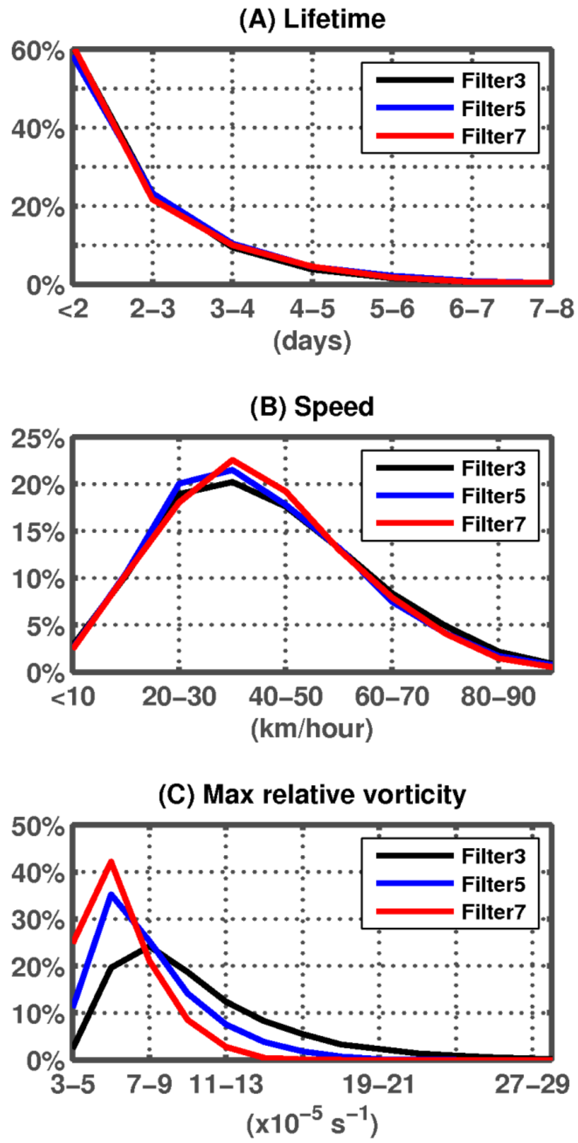

Figure 7 A) Relative frequency distributions of cyclones life times for the three sensitivity tests. B) As in A) but for cyclones average speed. C) as in A) but for tracks maximum relative vorticity D) as in C) but after excluding tracks that did not reach 10.7 and 5.8 of $x10^{-5}$ s^{-1} of relative vorticity in *filter3* and *filter5*, respectively.

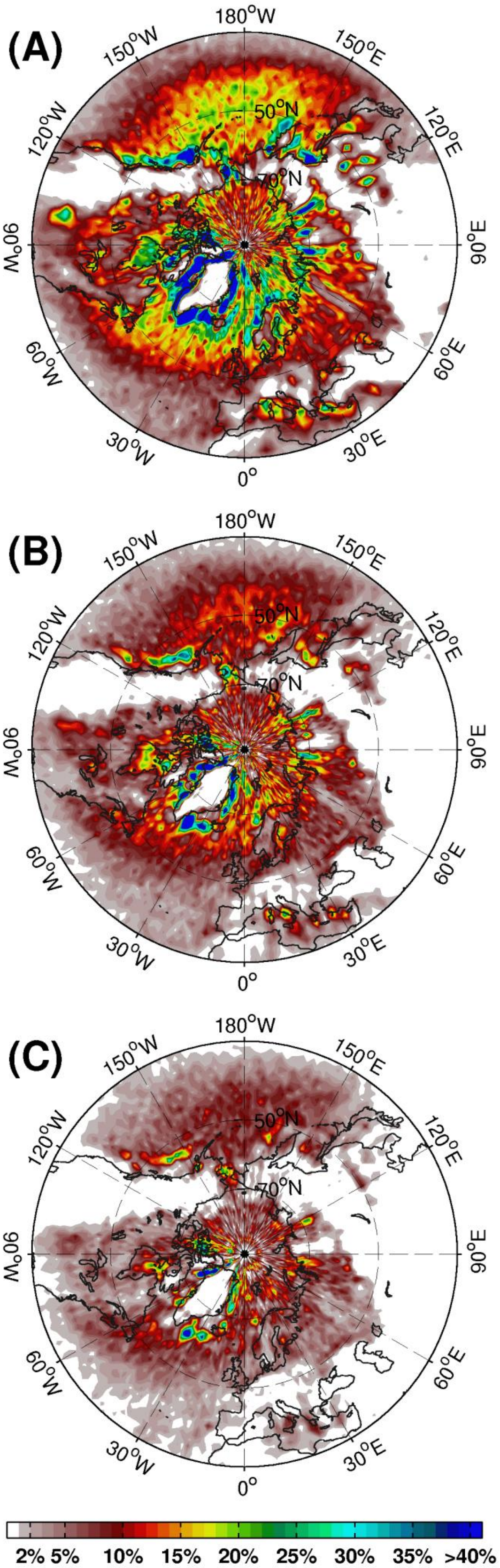

Figure 8 Cyclone center density expressed as the percentage of cyclone occurrence per time step and per unit area of (1000 km^2) for the A) *filter3*, B) *filter5* and C) *filter7*.

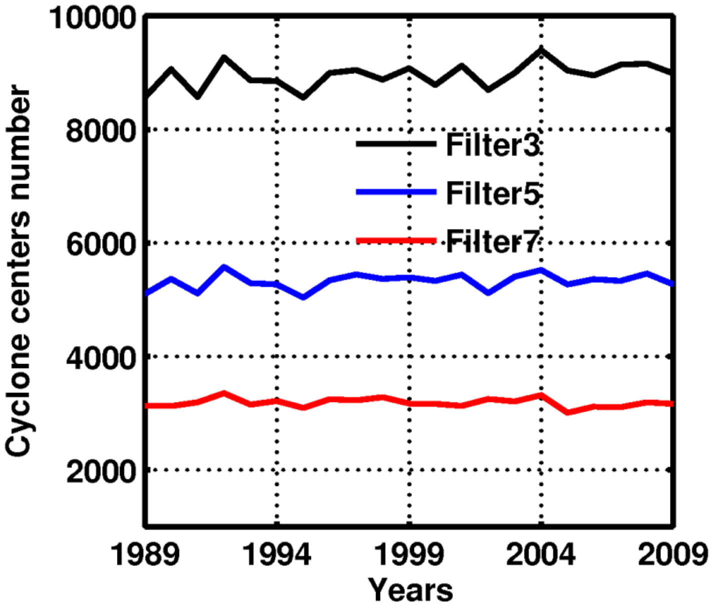

Figure 9 Number of cyclone centers as function of the year for the three sensitivity tests.

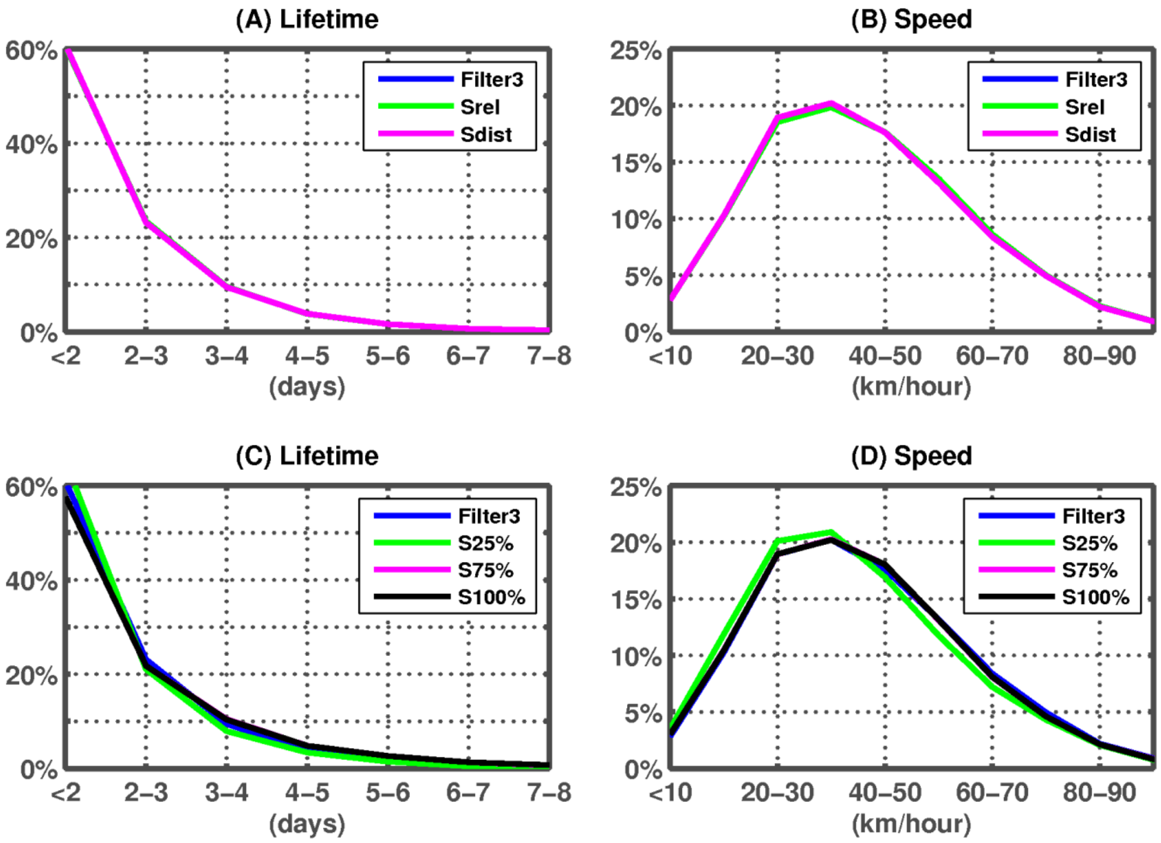

Figure 10 A) Relative frequency distribution of cyclones life time for the sensitivity tests *filter3*, S_{rel} and S_{dist}. B) As in A) but for cyclones average speed. C) as in (A) but for the sensitivity tests *filter3*, $S_{25\%}$, $S_{75\%}$ and $S_{100\%}$ D) as in (B) but for the sensitivity tests *filter3*, $S_{25\%}$, $S_{75\%}$ and $S_{100\%}$

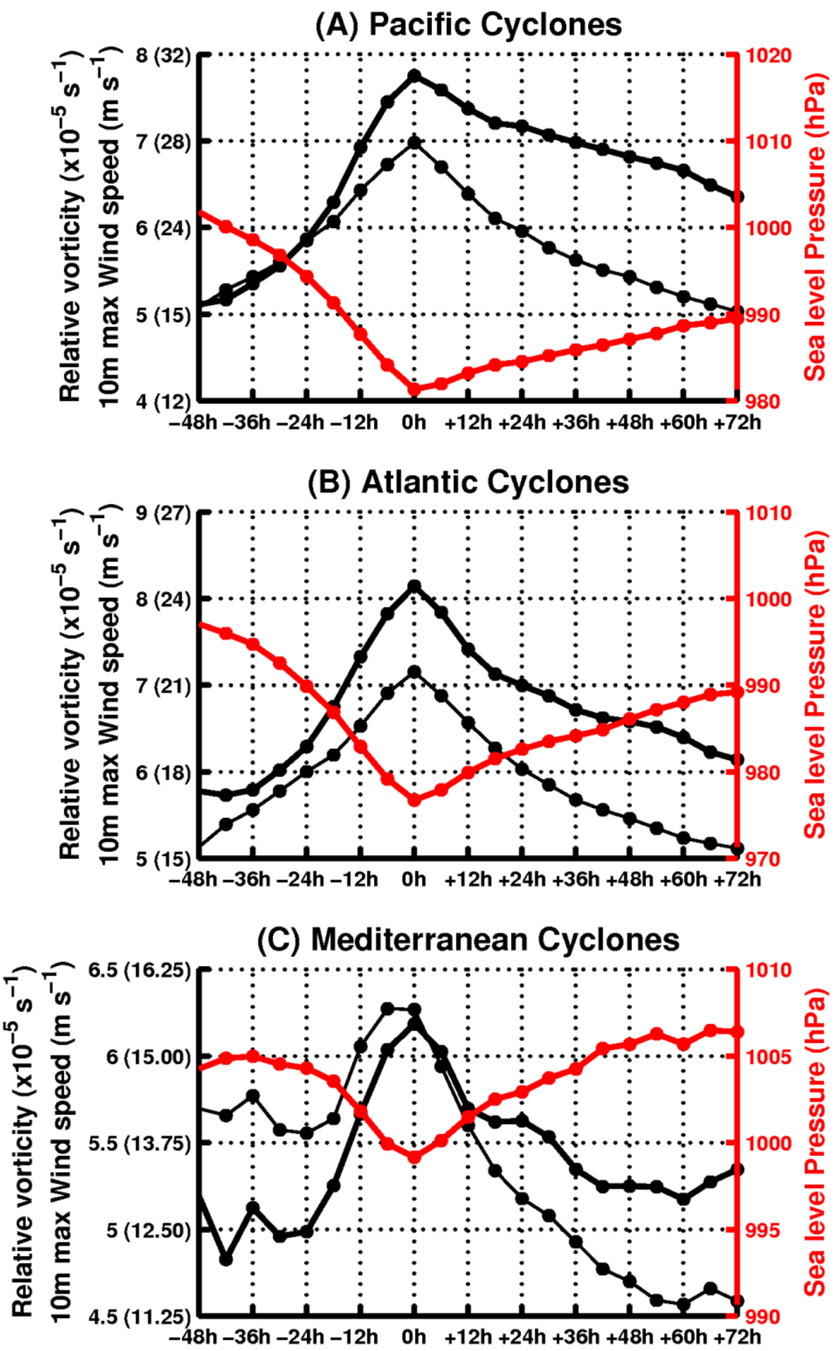

Figure 11 (A) Average composite time series of Pacific cyclones physical characteristics. 0h corresponds to the time when the cyclone presents its maximum relative vorticity: relative vorticity (thick black line), sea level pressure (red thick line) and maximum 10-meter wind speed (thin black line). Wind speed scale values are shown in the left vertical axes in parenthesis. (B) as in (A) for the Atlantic cyclones. (C) as in (A) for Mediterranean cyclones. Note that the Y-axis has not the same value intervals in the three panels.